Available online at www.sciencedirect.com
ScienceDirect
Clinical Biomechanics 23 (2008) 1269–1278
CLINICAL BIOMECHANICS
www.elsevier.com/locate/clinbiomech

Internal femoral forces and moments during running: Implications for stress fracture development

W. Brent Edwards [a,*], Jason C. Gillette [a], Joshua M. Thomas [b], Timothy R. Derrick [a]

[a] Department of Kinesiology, 283 Forker Building, Iowa State University, Ames, IA 50011-1160, USA
[b] Human Performance and Wellness Department, Trinity International University, Deerfield, IL 60015, USA

Received 23 February 2008; accepted 30 June 2008

Abstract

Background. Femoral stress fractures tend to occur at the neck, medial proximal-shaft, and distal-shaft. The purpose of this study was to determine the internal femoral forces and moments during running. It was expected that larger loads would occur at these common sites of femoral stress fracture.

Methods. Ten subjects ran at their preferred running speed over a force platform while motion capture data were collected. Static optimization in conjunction with a SIMM musculoskeletal model was used to determine individual muscle forces of the lower extremity. Joint contact forces were determined, and a quasi-static approach was used to calculate internal forces and moments along a centroid path through the femur.

Findings. The largest mean peak loads were observed at the following regions: anterior–posterior shear, 7.47 bodyweights (BW) at the distal-shaft (posteriorly directed); axial force, 11.40 BW at the distal-shaft (compression); medial–lateral shear, 3.75 BW at the neck (medially directed); anterior–posterior moment, 0.42 BW m at the proximal-shaft (medial surface compression); torsional moment, 0.20 BW m at the distal-shaft (external rotation); medial–lateral moment, 0.44 BW m at the distal-shaft (anterior surface compression).

Interpretation. The mechanical loading environment of the femur during running appears to explain well the redundancy in femoral stress fracture location. We observed the largest internal loads at the three femoral sites prone to stress fracture.

Keywords: Stress fracture; Joint contact forces; Internal bone loading; Musculoskeletal model

1. Introduction

Stress fractures result from repetitive cyclical loading of the skeletal system. Over time the bone fatigues and microdamage manifests as small cracks in the bony matrix (Burr et al., 1985). If the accumulation of microdamage exceeds the rate of bone repair, a stress fracture will result (Burr et al., 1990). Stress fractures commonly occur in the tibia and metatarsals (Korpelainen et al., 2001; Milgrom et al., 1985), but the femur accounts for approximately 10–33% of all stress fractures in military recruits (Finestone et al., 1991; Rauh et al., 2006) and approximately 4–14% in runners (McBryde, 1985; Sullivan et al., 1984).

In spite of the low relative occurrence of femoral stress fractures, they are among the most serious of overuse injuries. Several months of reduced weight-bearing or non-ambulatory activities may be necessary before training can be resumed (Ivkovic et al., 2006; Pihlajamäki et al., 2006b). Early detection is critical, as certain femoral stress fractures have a tendency to displace and require surgical fixation (Lee et al., 2003; Visuri et al., 1988). Any tissue damage resulting from the fracture itself, as well as perioperative trauma can lead to avascular necrosis, osteoarthritis, and in some instances permanent handicap (Lee et al., 2003; Visuri et al., 1988; Pihlajamäki et al., 2006a).

* Corresponding author.
E-mail address: edwards9@iastate.edu (W.B. Edwards).

0268-0033/$ - see front matter © 2008 Elsevier Ltd. All rights reserved.
doi:10.1016/j.clinbiomech.2008.06.011

There are three femoral locations that are particularly susceptible to stress fracture. Approximately 50% of all femoral stress fractures occur at the neck (McBryde, 1985; Niva et al., 2005). This is followed by a relatively high incidence of proximal-shaft fractures in runners that primarily occur on the medial surface (Butler et al., 1982; Hershman et al., 1990; Korpelainen et al., 2001; Lombardo and Benson, 1982), and distal-shaft fractures in military personnel that occur between distal one-third and femoral condyles (Giladi et al., 1986; Milgrom et al., 1985; Niva et al., 2005; Schmidt-Brudvig, 1985). Previous models of femoral loading fall short of identifying why femoral stress fractures occur in these locations. In part, this may be due to the complex nature of bone loading and the simplifications used when modeling gait. However, even in the most complex of models (Duda et al., 1998; Polgár et al., 2003), extrapolation of the results to running is difficult because joint contact and muscle force inputs are often based on walking.

Traditionally, external reaction forces have been used to experimentally investigate the relationship between mechanical loading and stress fracture development (Bennell et al., 2004; Milner et al., 2006b). Although running ground reaction forces typically range between 2 and 3 body weights (BW) (Munro et al., 1987), they comprise only a small portion of the skeletal loading environment. Results from instrumented hip prostheses suggest that muscle forces contribute an additional 3 BW of force during slow jogging (1.1–2.2 m/s) (Bergmann et al., 1993). A recent modeling study estimated that muscles crossing the ankle joint contribute an additional 7 BW of force during running (3.5–4.0 m/s) (Sasimontonkul et al., 2007). Furthermore, the stresses arising from axially oriented muscle loading is small when compared to the stresses on the periphery of the bone due to bending (Biewener et al., 1983).

The purpose of this study was to determine internal femoral loads during running. A combination of experimental and modeling techniques were used to calculate three orthogonal forces and three orthogonal moments acting at 11 equidistant points along the length of the femur. It was expected that the largest internal femoral forces and moments would occur at common sites of femoral stress fracture reported in the literature.

2. Methods

2.1. Subjects

Ten experienced male runners (six rear-foot strikers, four fore-foot strikers) were recruited for this study (age 22.20 ± 3.16 years, height 1.78 ± 0.05 m, mass 69.15 ± 6.48 kg). At the time of data collection subjects were free from lower extremity injury and ran more than 20 miles/week. Prior to participation, subjects gave written informed consent and the study was approved by the Iowa State University Human Subjects Review Board.

2.2. Data collection

Upon arrival, each subject was outfitted with a standardized commercially available running shoe, a black spandex shirt, and black spandex shorts. A series of anthropometric measurements were taken and 13 retroreflective markers were placed on anatomical landmarks of the trunk and right lower extremity. All anthropometric measurements and retroreflective marker placements were performed by the same researcher.

Preferred running speed was determined over a series of practice trials, during which the subjects ran along the 28.5 m runway of the lab. The subjects were asked to aim for a speed they would select for an 8–10 mile recovery run. Running speed was monitored with motion capture and the average value of 3–4 practice trials within a range of 5% was considered the preferred running speed.

Subjects ran at their preferred running speed (4.43 ± 0.48 m/s) over a force platform (AMTI, Watertown, MA) until ten successful trials were completed. Trials were accepted if the speed was $\pm 5\%$ of their preferred running speed and the subject's right foot hit the force platform with no visually identified targeting. Motion-capture data were collected with a Peak Motus 3D optical capture system (Vicon Peak, Centennial, CO) at a sampling frequency of 120 Hz. Force platform data were collected concurrently at a sampling frequency of 1200 Hz. The synchronized raw motion-capture and force platform data were then exported to Matlab (The Mathworks, Natick, MA) for processing.

2.3. Data processing

The raw motion capture data were interpolated to 1200 Hz using a cubic spline technique and then smoothed using a low-pass zero-lag Butterworth filter with a cutoff frequency of 8 Hz. Ground reaction force data were also smoothed in the same manner with a cutoff frequency of 50 Hz. A static trial was used to estimate joint center locations which were assumed to be stationary in the segmental coordinate systems. Three-dimensional Cardan segment and joint angles were then calculated with a flexion/extension, abduction/adduction, internal/external rotation sequence.

Segment masses, center of mass locations, and moments of inertia were obtained according to Vaughan et al. (1992), using anthropometric measurements acquired prior to data collection. Joint moments and reaction forces were calculated using inverse dynamics and rigid body assumptions. Values were transformed to the distal segment coordinate system of each joint. The segment coordinate systems were described using a right handed rule, with the x-axis oriented in the anterior–posterior (AP) direction, the y-axis oriented in the axial direction, and the z-axis oriented in the medial–lateral (ML) direction.

The stance phase joint angles for each trial were interpolated to percentage of stance (1% increments) and imported

into a scaled SIMM 4.0 musculoskeletal model (MusculoGraphics Inc., Santa Rosa, CA). The reader is referred to Delp and Loan (1995) for a detailed overview of the musculoskeletal modeling software. The SIMM model was used to obtain dynamic maximal muscle forces, muscle moment arms, and muscle orientations for 43 lower extremity muscles. The maximum dynamic muscle forces were adjusted for length and velocity. The information provided by SIMM was then re-imported into Matlab for the estimation of individual muscle forces.

Muscle forces were optimized using the *fmincon* function in Matlab. The *fmincon* function uses sequential quadratic programming; it begins with an initial guess and searches the solution space in the direction of 'steepest descent' such that the magnitude of the cost function is decreased. The cost function (u) to be minimized was the sum of squared muscle stresses (Glitsch and Baumann, 1997):

$$u = \sum_{i=1}^{43} \left(\frac{f_i}{\mathrm{PCSA}_i} \right)^2$$

where f_i is the force generated by the ith muscle, and PCSA_i is the physiological cross-sectional area of the ith muscle. The optimization was constrained so that the resulting hip, knee, and ankle moments equaled those from inverse dynamics. Five moments were utilized in the optimization procedure including three orthogonal components (j) of the resultant moment at the hip, and one (flexion–extension) component at the knee and ankle:

$$M_j^{\mathrm{h}} = \sum_{i=1}^{27} r_i^{\mathrm{h}} \times f_i \quad j = x, y, z$$

$$M_z^{\mathrm{k}} = \sum_{i=21}^{33} r_i^{\mathrm{k}} \times f_i$$

$$M_z^{\mathrm{a}} = \sum_{i=31}^{43} r_i^{\mathrm{a}} \times f_i$$

where M^{h}, M^{k}, and M^{a} are the three components of the resultant moment at the hip, and one component each of the resultant moment at the knee and ankle, respectively, and r^{h}, r^{k}, and r^{a} are the muscle moment arms about the hip, knee, and ankle, respectively. The lower bound muscle forces were initially set to zero and the upper bound muscle forces were initially set to the maximal dynamic muscle forces obtained from SIMM. The bounds were then adjusted in subsequent frames to prevent non-physiological changes in muscle force (Pierrynowski and Morrison, 1985):

$$lb_i = q - \left(1 - \mathrm{e}^{-\mathrm{d}t/t_{\mathrm{down}}}\right) \times q$$

$$ub_i = q + \left(1 - \mathrm{e}^{-\mathrm{d}t/t_{\mathrm{up}}}\right) \times (1 - q)$$

where lb_i and ub_i are the lower and upper bounds for the ith muscle, $q = f_i$ divided by the respective maximal dynamic muscle force, $\mathrm{d}t$ is the time step, $t_{\mathrm{down}} = 0.034$ s, and $t_{\mathrm{up}} = 0.003$ s. If the predicted muscle force went beyond its bound it was penalized within the cost function such that:

$$lb\mathrm{pen}_i = 0 \quad (f_i \geqslant lb_i)$$

$$lb\mathrm{pen}_i = \left[\frac{(lb_i - f_i)}{\mathrm{PCSA}_i} \right]^2 \quad (f_i < lb_i)$$

$$ub\mathrm{pen}_i = 0 \quad (f_i \leqslant ub_i)$$

$$ub\mathrm{pen}_i = \left[\frac{(f_i - ub_i)}{\mathrm{PCSA}_i} \right]^2 \quad (f_i > ub_i)$$

$$u' = \sum_{i=1}^{43} \left(\frac{f_i}{\mathrm{PCSA}_i} \right)^2 + lb\mathrm{pen}_i + ub\mathrm{pen}_i$$

where $lb\mathrm{pen}_i$ and $ub\mathrm{pen}_i$ are the penalties for the ith muscle force, and u' is the cost function adjusted for the penalty.

Three-dimensional joint contact forces were calculated as the sum of reaction force and muscle forces crossing the joint. Joint contact forces were referenced to the local coordinate system of the distal segment

$$Fc_j^{\mathrm{h}} = \left[RF_j^{\mathrm{h}} + \sum_{i=1}^{27} f_{ij} \right] \quad j = x, y, z$$

$$Fc_j^{\mathrm{k}} = \left[RF_j^{\mathrm{k}} + \sum_{i=21}^{33} f_{ij} \right] \quad j = x, y, z$$

where Fc^{h} and Fc^{k} are the three components of the joint contact force at the hip and knee, respectively, RF^{h} and RF^{k} the three components of the joint reaction forces at the hip and knee, respectively, and f_{ij} are the three components of the ith predicted muscle force crossing the respective joint. The patella–femoral contact force was calculated as the resultant of the quadriceps and patella ligament forces assuming a ratio of 1:1.

Internal forces and moments of the femur were calculated in a similar manner to Duda et al. (1997). The calculations were based on a quasi-static equilibrium of forces and moments at each 1% of the stance phase. The overall equilibrium of the femur was described as

$$\sum_{i=1}^{33} f_i + Fc^{\mathrm{h}} + Fc^{\mathrm{k}} + Fc^{\mathrm{p}} + G = 0$$

$$\sum_{i=1}^{33} r_i \times f_i + rc^{\mathrm{h}} \times Fc^{\mathrm{h}} + rc^{\mathrm{k}} \times Fc^{\mathrm{k}} + rc^{\mathrm{p}} \times Fc^{\mathrm{p}} + g \times G = 0$$

where Fc^{p} is patella–femoral contact force, G is the weight of the thigh, and r, rc^{h}, rc^{k}, rc^{p}, and g are the corresponding moments arms to the muscle force, hip contact force, knee contact force, patella–femoral contact force, and weight component, respectively.

Internal forces and moments were calculated along a centroid path at 11 equidistant points within the femur, beginning at the femoral neck (Fig. 1). The vertices defining the femur of the musculoskeletal model were used as a basis for the calculation of centroid path. The loading environment at each point was determined by assuring equilibrium with all forces acting on the section above. Internal

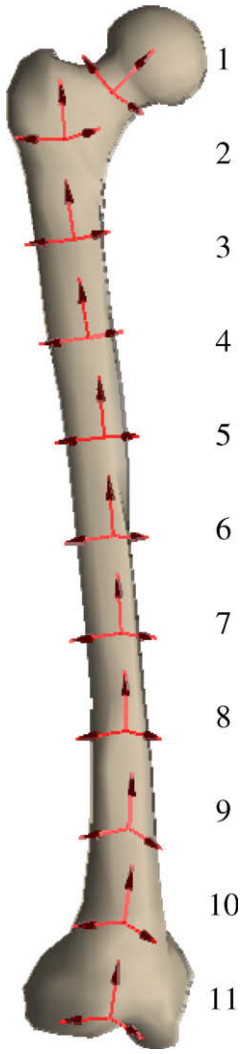

Fig. 1. Local-internal femoral coordinate systems for 11 points along a centroid path of the femur. View is approximately 45° between frontal and sagittal plane.

forces and corresponding moments were calculated in the thigh coordinate system and then rotated into their respective local-internal femoral coordinate systems. The axial component of the local-internal femoral coordinate systems were described by an axially oriented vector extending towards the point above. The AP axes were calculated as the cross product of the local-internal femoral axial axes and the thigh ML axis. The ML axes were calculated as the cross product of the local-internal femoral axial axes and the local-internal femoral AP axes. The thigh weight component was assumed to be linearly distributed extending from the center of mass towards the proximal and distal ends of the femur.

All data were normalized to BW and analyzed descriptively. Peak internal femoral forces and moments and their time of occurrence were calculated and the mean and standard deviation across subjects was determined. In this paper the first 30% of stance is referred to as the impact phase and the later 70% is referred to as the active phase.

3. Results

3.1. Joint moments

The joint reaction forces and moments obtained from inverse dynamics are displayed in Fig. 2. The axial oriented reaction forces were large in comparison to the AP and ML reaction forces. The sagittal plane moments were primarily extensor, with peak magnitudes occurring near midstance for the knee and ankle, and during the impact phase for the hip. In addition, a relatively large abduction moment was observed at the hip and knee, and a relatively large inversion moment at the ankle.

3.2. Muscle forces

Ensemble average muscle forces for representative muscle groups are displayed in Fig. 3. The prominent hip extensors, knee extensors, and ankle extensors tended to follow the general trend of the joint moments. The largest muscle forces were created by the knee extensors. Similar to the joint moments, peak vasti (VAS), rectus femoris (RF), gastrocnemius (GAS), and soleus (SOL) occurred near midstance while peak gluteus maximus (GMAX) activity occurred earlier in stance. Some hamstring (HAM) and tibialis anterior (TA) muscle activity was observed at both early and late stance.

3.3. Joint contact forces

The axial joint contact forces were compressive and large in relation to the other components of the joint contact force (Fig. 4). The peak AP joint contact force acted in the posterior direction at the hip (-1.60 ± 0.45 BW) and knee (-1.83 ± 0.08 BW). Peak axial forces were larger at the knee (-15.09 ± 0.59 BW) than at the hip (-11.89 ± 2.19 BW). The peak ML joint contact force acted in the lateral direction at the hip (6.25 ± 0.83 BW) and in the medial direction at the knee (-1.19 ± 0.07 BW). The mean peak resultant patella–femoral contact force was 7.09 ± 0.27 BW.

3.4. Internal femoral forces

The internal forces at 11 equidistant points along the femur are displayed in Fig. 5. Point 1 corresponds to the most proximal point analyzed (at the femoral neck) and point 11 corresponds to the most distal point analyzed (at the femoral condyles). Prominent AP shear forces were observed at the proximal and distal ends of the femur. Mean peak AP forces ranged from 3.57 BW at point 1 to −7.47 BW at point 11 (Table 1). The anteriorly oriented force at point 1 occurred during the impact phase, while the posteriorly oriented force at point 11 occurred during the active phase near midstance.

The axial oriented forces were larger than the AP and ML forces at each point within the femur. Mean peak axial forces ranged from −6.79 BW at point 1 to −11.40 BW at

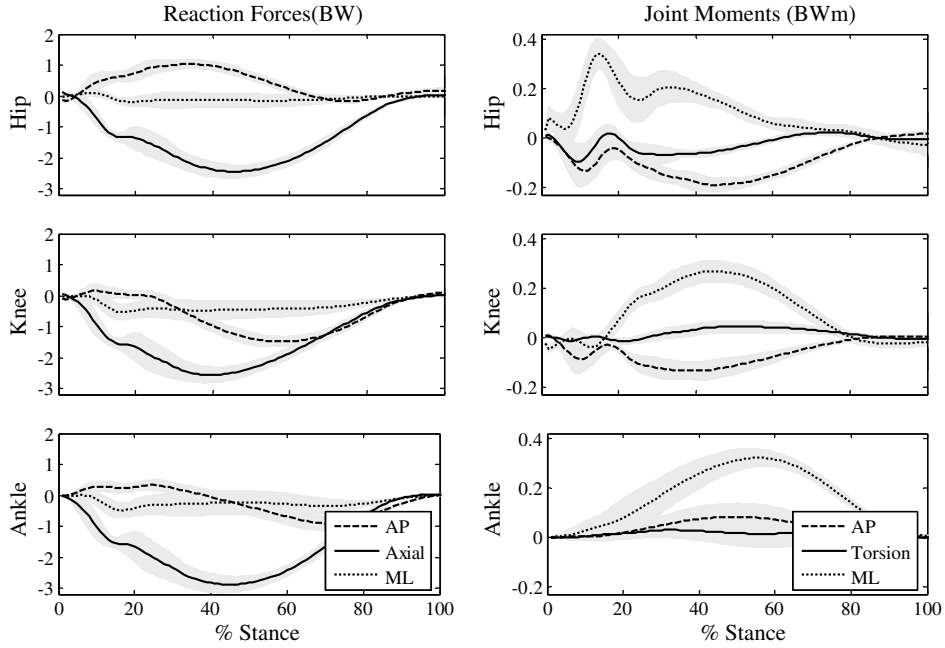

Fig. 2. Ensemble average joint reaction forces and moments calculated from inverse dynamics. Positive reaction forces are directed anterior, upward, and lateral. Positive moments correspond to adduction, internal rotation, and extension.

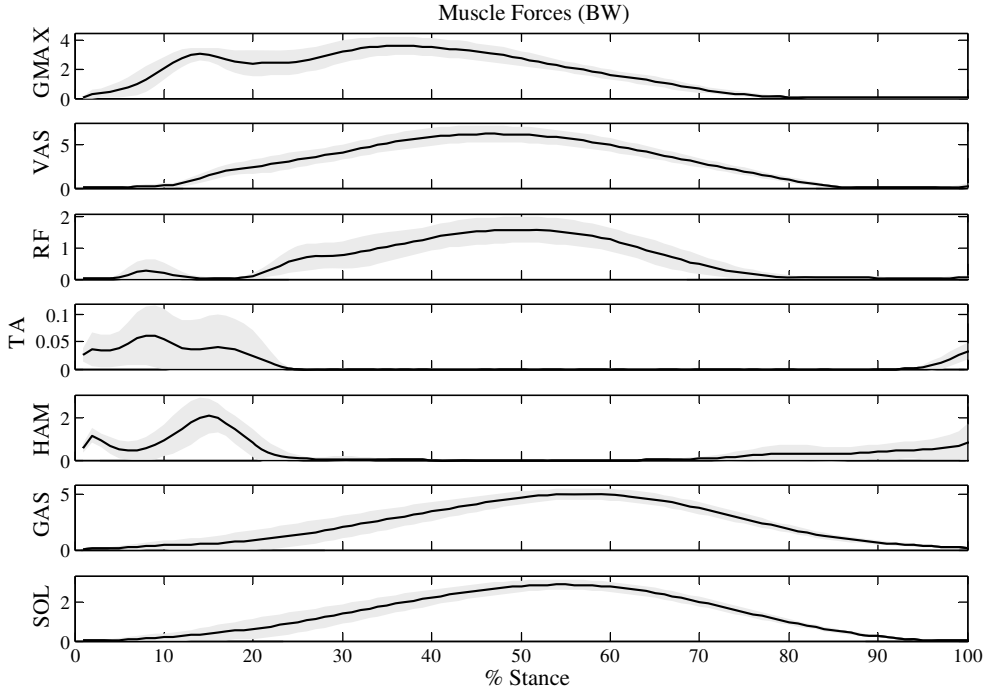

Fig. 3. Ensemble average muscle forces for representative muscle groups calculated from computer optimization (GMAX, gluteus maximus; VAS, vasti muscles; RF, rectus femoris; TA, tibialis anterior; HAM, hamstring muscles; GAS, gastrocnemius; SOL, soleus).

point 11. Peak axial forces at the proximal femur occurred during the impact phase, while those at the middle and distal femur occurred during the active phase closer to midstance.

A prominent ML shear force was observed at the proximal femur. Mean peak ML forces ranged from 2.23 BW at point 3 to −3.75 BW at point 1. The medially oriented force at point 1 occurred during the impact phase, while all other peak ML shear forces occurred during the beginning of the active phase.

3.5. Internal femoral moments

The internal moments at 11 equidistant points along the femur are displayed in Fig. 5. Large bending moments

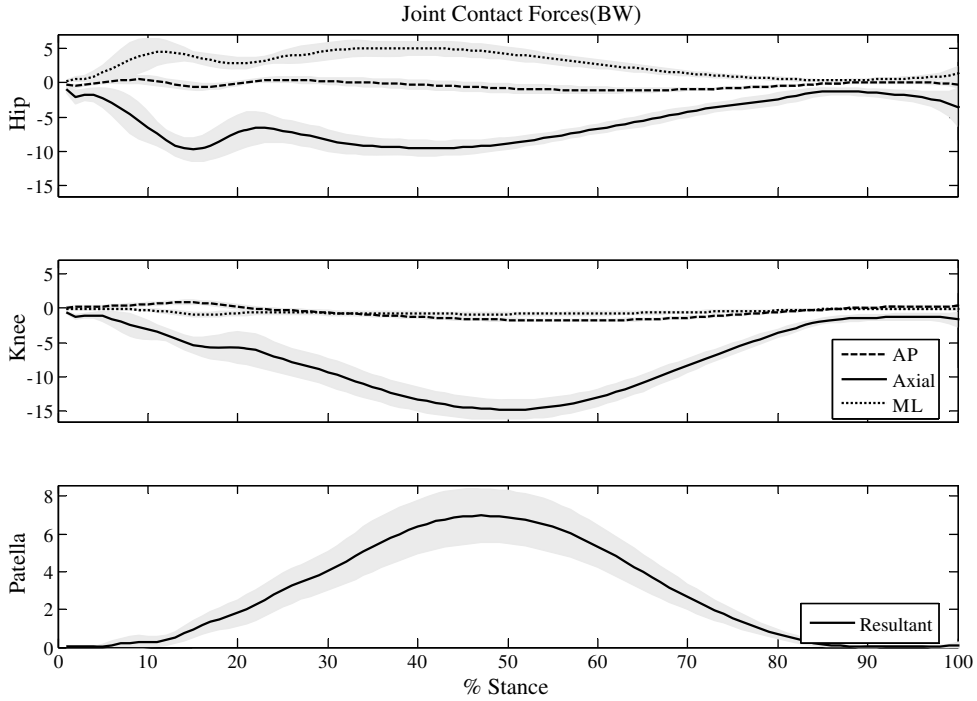

Fig. 4. Ensemble average joint contact forces at the hip and knee. Positive contact forces are directed anterior, upward, and lateral.

about the AP axis were observed during the impact and active phase. The peak AP moments during impact were negative, signifying compression on the medial surface of the femur and tension on the lateral-surface of the femur. The peak AP moments during the active phase were negative at the proximal end of the femur and positive at the distal end of the femur. The mean peak AP moments ranged from 0.31 BW m at point 11 to −0.42 BW m at point 2 (Table 2).

The torsional moments were small compared to the AP and ML bending moments. Apart from points 2 and 3, mean peak torsional moments occurred during the impact phase of running. The peak torsional moments would cause internal rotation at the proximal femur and external rotation at the middle and distal femur. The mean peak torsional moments ranged from 0.15 BW m at point 2 to −0.20 BW m at point 11.

Large ML bending moments were observed during the impact phase and active phase. The peak ML bending moments were all negative signifying compression on the anterior surface of the femur and tension on the posterior surface of the femur. At the proximal femur the peak ML bending moments occurred during impact, but occurred during the active phase at the middle and distal femur. The mean peak ML moments ranged from −0.20 BW m at points 1, 5, and 6 to −0.44 BW m at point 11.

4. Discussion

The purpose of this study was to determine the internal femoral forces and moments during running, and to find out if larger loads occurred at common sites of femoral stress fracture. The results of our study suggest that frequently cited locations of femoral stress fracture do experience larger loads relative to the rest of the femur.

The etiology of stress fractures is multifactorial and contributing risk factors can be categorized as being either extrinsic (e.g., surface, athletic footwear, training regime) or intrinsic (e.g., bone strength, bone fatigability, bone turnover rate) (Bennell et al., 1999). The combination of risk factors has the potential to vary between each stress fracture occurrence, but it is the interaction of these risk factors with the mechanical loading environment that ultimately leads to injury. The subsequent paragraphs suggest a biomechanical relationship between the loading environment and frequently cited locations of femoral stress fracture.

The femoral neck is subjected to large anteriorly and medially oriented shear forces during running. These shear forces occur early on in stance and are likely related to the breaking force that occurs following heel-strike. Although axial forces and moments at the neck were no larger than those experienced by the rest of the femur, peak loads always occurred during the impact phase of running. The impact phase of running is associated with a high rate of loading, and microdamage to cortical bone increases proportionally to loading rate (Schaffler et al., 1989). Over time, this type of loading combined with the small diameter of the femoral neck may pose a threat to skeletal integrity.

Femoral stress fractures at the proximal-shaft tend to occur on the medial aspect of the femur (Butler et al., 1982; Hershman et al., 1990; Lombardo and Benson, 1982). We found the largest bending moments about the

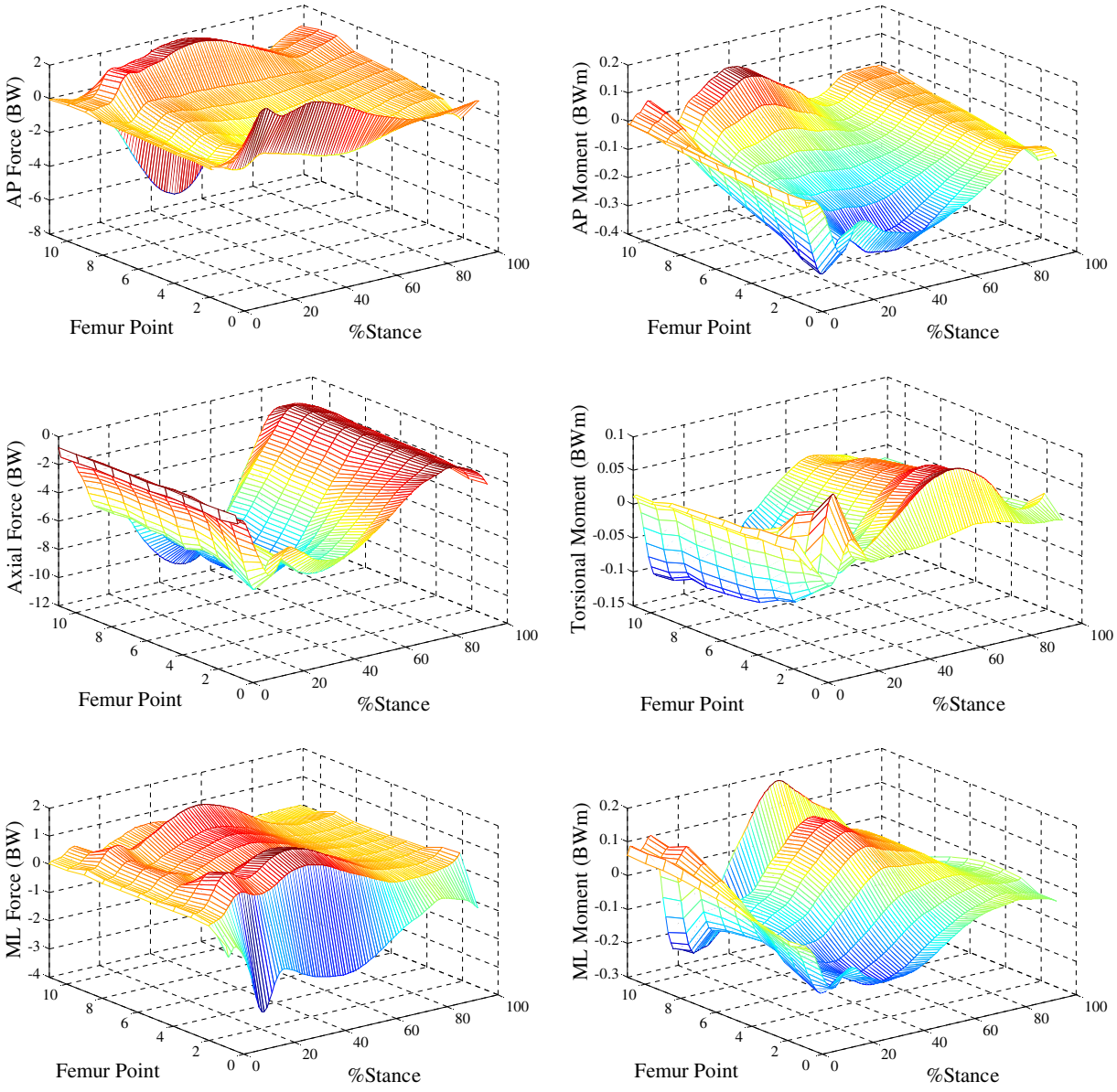

Fig. 5. Ensemble average internal forces and moments at the femur. Positive internal forces correspond to anterior shear, tension, and lateral shear. Positive internal moments correspond to lateral-surface compression, internal-rotation torsion, and posterior-surface compression.

AP axes at the proximal femur during the impact phase of loading. The direction of this bending moment in conjunction with the axially oriented compressive force would place the largest normal stress on the medial aspect of the femur. As cortical bone is strongest in compression (Reilly and Burstein, 1975), the reason that proximal-shaft fractures materialize on the medial surface is unclear. It is possible that in an *in vivo* situation the difference between medial surface compressive stress and lateral-surface tensile stress outweighs the difference in anisotropic strength. These differences may become even more pronounced with training when the muscles that resist the AP bending moment (hip abductors) begin to fatigue.

The largest AP shear, axial forces, and ML bending moments were observed at the distal femur near the femoral condyle. Peak loads occurred during midstance and were associated with peak patella–femoral contact force and peak muscular force of the quadriceps and gastrocnemius. In addition, the largest torsional moment was observed at the distal femur, and in-phase combined torsion and axial loading has been shown to cause a sevenfold reduction in cortical bone fatigue life (George and Vashishth, 2005). Recently, the free moment, a vertically oriented torque experienced between the foot and ground, was found to be a strong predictor of subjects with a history of tibial stress fracture (Milner et al., 2006a). It is unclear how influential the free moment is on the torsional moment experienced throughout the femur, but it appears that torsional type loading may play an important role in stress fracture development.

Published research on the internal loading environment of the femur during running is sparse. Internal femoral

Table 1
Mean (SD) peak internal femoral force magnitudes and % stance of occurrence for all subjects and all trials

Femur point	AP force		Axial force		ML force	
	Magnitude (BW)	% Stance	Magnitude (BW)	% Stance	Magnitude (BW)	% Stance
1	3.57 (0.14)	22.32 (2.50)	−6.79 (1.33)	25.04 (9.04)	−3.75 (0.32)	20.58 (4.84)
2	−1.91 (0.83)	41.71 (12.13)	−8.40 (0.92)	22.28 (5.23)	1.94 (0.61)	36.53 (7.18)
3	−1.78 (0.43)	38.57 (10.76)	−8.12 (0.79)	27.80 (5.27)	2.23 (0.52)	36.10 (7.8)
4	−1.97 (0.13)	34.92 (8.79)	−8.01 (0.51)	34.02 (5.40)	1.87 (0.14)	33.70 (5.25)
5	−1.62 (0.08)	28.08 (6.02)	−8.66 (0.60)	39.79 (5.19)	1.32 (0.15)	35.98 (10.33)
6	−1.27 (0.09)	25.50 (5.35)	−9.98 (0.64)	41.58 (4.51)	1.50 (0.15)	36.14 (10.42)
7	−1.03 (0.09)	21.58 (3.21)	−9.84 (0.67)	43.21 (4.82)	1.52 (0.16)	37.82 (10.28)
8	1.15 (0.09)	53.24 (9.08)	−9.84 (0.67)	43.25 (4.83)	1.52 (0.16)	37.85 (10.27)
9	3.04 (0.17)	36.97 (5.26)	−9.37 (0.64)	43.61 (4.97)	1.99 (0.19)	39.35 (8.63)
10	2.77 (0.16)	36.67 (4.42)	−9.59 (0.66)	43.92 (4.98)	1.06 (0.11)	33.30 (10.77)
11	−7.47 (0.22)	48.95 (3.73)	−11.40 (0.64)	49.41 (4.23)	1.32 (0.14)	32.00 (6.20)

Table 2
Mean (SD) peak internal femoral moment magnitudes and % stance of occurrence for all subjects and all trials

Femur point	AP moment		Torsional moment		ML moment	
	Magnitude (BW m)	% Stance	Magnitude (BW m)	% Stance	Magnitude (BW m)	% Stance
1	−0.31 (0.06)	24.65 (6.32)	0.05 (0.01)	17.61 (2.84)	−0.20 (0.02)	23.23 (3.58)
2	−0.42 (0.07)	22.00 (6.66)	0.15 (0.02)	31.28 (8.12)	−0.22 (0.01)	25.06 (4.33)
3	−0.39 (0.04)	22.33 (4.00)	0.11 (0.02)	40.37 (9.18)	−0.22 (0.01)	26.84 (3.67)
4	−0.34 (0.02)	22.97 (3.80)	−0.12 (0.01)	19.56 (4.30)	−0.22 (0.01)	26.30 (3.51)
5	−0.33 (0.02)	24.03 (3.57)	−0.14 (0.01)	18.02 (3.78)	−0.20 (0.02)	25.66 (2.73)
6	−0.32 (0.02)	24.56 (3.07)	−0.15 (0.01)	18.16 (3.76)	−0.20 (0.02)	34.59 (4.97)
7	−0.31 (0.02)	25.94 (3.42)	−0.16 (0.01)	18.61 (3.49)	−0.22 (0.03)	37.90 (6.06)
8	−0.30 (0.03)	27.43 (4.41)	−0.16 (0.01)	18.67 (3.60)	−0.26 (0.03)	39.31 (6.72)
9	−0.29 (0.03)	28.47 (4.92)	−0.19 (0.01)	20.54 (5.15)	−0.30 (0.04)	43.24 (7.87)
10	0.27 (0.03)	34.70 (8.01)	−0.18 (0.01)	19.84 (4.37)	−0.42 (0.04)	40.23 (6.76)
11	0.31 (0.04)	34.00 (7.64)	−0.20 (0.01)	21.89 (4.55)	−0.44 (0.05)	41.58 (8.30)

loads have been directly measured during slow jogging by way of an instrumented femoral replacement (Taylor and Walker, 2001). Forces and moments were telemetered from a location approximating the mid-femur. Peak loads averaging −3.3 BW, −0.08 BW m, −0.01 BW m, and −0.06 BW m were reported for axial force, the AP moment, torsion moment, and ML moment, respectively. Although the directions of these loads are in agreement with our analysis, the magnitudes are on average less than half the peak loads estimated at the mid-femur in this study. Several explanations can be given for this discrepancy. First, the slow jogging speed of 1.8 m/s reported by Taylor and Walker (2001), is below that consistently reported for the walk to run gait transition (2.0 m/s) (Diedrich and Warren, 1995; Hreljac, 1993), and may therefore be more closely related to a brisk walk. Our subjects' preferred running speed averaged 4.4 m/s, and many loading characteristics during running are more than double those found during walking, such as ground reaction forces and net internal joint moments (Novacheck, 1998). Second, while Taylor and Walker (2001) mention that internal forces from an instrumented femoral replacement may be lower than normal due to reductions and losses in muscle function, the static optimization procedure we used to determine muscle forces has been criticized for over-predicting muscle force magnitudes (Prilutsky et al., 1997). Therefore, it is possible that the internal loads calculated in this study are slightly overestimated. Nevertheless, static optimization shows close agreement to EMG patterns during locomotion (Crowninshield and Brand, 1981; Heintz and Gutierrez-Farewik, 2007), and compares well with dynamic optimization solutions (Anderson and Pandy, 2001). In addition, the experimental joint moments used to constrain our optimized muscle forces agree well with previous running literature (Derrick et al., 1998; Pollard et al., 2004).

Equally important to the limitations of static optimization are the limitations associated with our generic musculoskeletal model. The model was linearly scaled to the length of each subject's segments, but this scaling did not account for subject variation in bone morphology. Differences in femoral anteversion and neck-shaft angle could influence the internal loading environment by altering the centroid path as well as muscle moment arms. Knowledge of inter individual bone geometry and strength would also improve our study. These parameters would allow for the estimation of skeletal stresses and strains which have a more direct relationship with stress fracture.

In conclusion, the mechanical loading environment of the femur explains well the redundancy in femur stress fracture location cited in the literature, i.e. the neck, medial proximal-shaft, and distal-shaft. Each of these locations experiences a relatively unique loading environment and it is quite possible that several different mechanisms are responsible for the development of femoral stress fracture. As these internal loads cannot be realized through measurement of external reaction forces, it may be necessary for future research to utilize the technique presented herein in order to better explain the correlation between mechanical loading and stress fracture development.

References

Anderson, F.C., Pandy, M.G., 2001. Static and dynamic optimization solutions for gait are practically equivalent. Journal of Biomechanics 34, 153–161.

Bennell, K., Matheson, G., Meeuwisse, W., Brukner, P., 1999. Risk factors for stress fractures. Sports Medicine 28, 91–122.

Bennell, K., Crossley, K., Jayarajan, J., Walton, E., Warden, S., Kiss, Z.S., Wrigley, T., 2004. Ground reaction forces and bone parameters in females with tibial stress fracture. Medicine and Science in Sports and Exercise 36, 397–404.

Bergmann, G., Graichen, F., Rohlmann, A., 1993. Hip joint loading during walking and running measured in two patients. Journal of Biomechanics 26, 969–990.

Biewener, A.A., Thomason, J., Goodship, A., Lanyon, L.E., 1983. Bone stress in the horse forelimb during locomotion at different gaits: a comparison of two experimental methods. Journal of Biomechanics 16, 1983.

Burr, D.B., Martin, R.B., Shaffler, M.B., Radin, E.L., 1985. Bone remodeling in response to in vivo fatigue microdamage. Journal of Biomechanics 18, 189–200.

Burr, D.B., Milgrom, C., Boyd, R.D., Higgins, W.L., Robin, G., Radin, E.L., 1990. Experimental stress fracture of the tibia. The Journal of Bone and Joint Surgery 72-B, 370–375.

Butler, J., Brown, S.L., Mcconnell, B.G., 1982. Subtrochanteric stress fracture in runners. American Journal of Sports Medicine 10, 228–232.

Crowninshield, R.D., Brand, R.A., 1981. A physiologically based criterion of muscle force prediction in locomotion. Journal of Biomechanics 14, 793–801.

Delp, S.L., Loan, J.P., 1995. A graphics-based software system to develop and analyze models of musculoskeletal structures. Computers in Biology and Medicine 25, 21–34.

Derrick, T.R., Hamill, J., Caldwell, G.E., 1998. Energy absorption of impacts during running at various stride lengths. Medicine and Science in Sports and Exercise 30, 128–135.

Diedrich, F.J., Warren, W.H., 1995. Why change gaits? Dynamics of walk-run transition. Journal of Experimental Psychology 21, 183–202.

Duda, G.N., Schneider, E., Chao, E.Y.S., 1997. Internal forces and moments in the femur during walking. Journal of Biomechanics 30, 933–941.

Duda, G.N., Heller, M., Albinger, J., Schulz, O., Schneider, E., Claes, L., 1998. Influence of muscle forces on femoral strain distribution. Journal of Biomechanics 31, 841–846.

Finestone, A., Shlamkovitch, N., Eldad, A., Wosk, J., Laor, A., Danon, Y.L., Milgrom, C., 1991. Risk factors for stress fractures among Israeli infantry recruits. Military Medicine 156, 528–530.

George, W., Vashishth, D., 2005. Influence of phase angle between axial and torsional loadings on fatigue fractures of bone. Journal of Biomechanics 38, 819–825.

Giladi, M., Milgrom, C., Kashtan, H., Stein, M., Chisin, R., Dizian, R., 1986. Recurrent stress fractures in military recruits. The Journal of Bone and Joint Surgery 68-B, 439–441.

Glitsch, U., Baumann, W., 1997. The three-dimensional determination of internal loads in the lower extremity. Journal of Biomechanics 30, 1123–1131.

Heintz, S., Gutierrez-Farewik, E.M., 2007. Static optimization of muscle forces during gait in comparison to EMG-to-force processing approach. Gait and Posture 26, 279–288.

Hershman, E.B., Lombardo, J., Bergfeld, J.A., 1990. Femoral shaft stress fractures in athletes. Clinics in Sports Medicine 9, 111–119.

Hreljac, A., 1993. Preferred and energetically optimal gait transition speeds in human locomotion. Medicine and Science in Sports and Exercise 25, 1158–1162.

Ivkovic, A., Bojanic, I., Pecina, M., 2006. Stress fractures of the femoral shaft in athletes: a new treatment algorithm. British Journal of Sports Medicine 40, 518–520.

Korpelainen, R., Orava, S., Karpakka, J., Siira, P., Hulkko, A., 2001. Risk factors for recurrent stress fracture in athletes. American Journal of Sports Medicine 29, 304–310.

Lee, C.-H., Huang, G.-S., Chao, K.-H., Jean, J.-L., 2003. Surgical treatment of displaced stress fractures of the femoral neck in military recruits: a report of 42 cases. Archives of Orthopaedic and Trauma Surgery 123, 527–533.

Lombardo, S.J., Benson, D.W., 1982. Stress fractures of the femur in runners. American Journal of Sports Medicine 10, 219–227.

McBryde, A.M., 1985. Stress fractures in runners. Clinics in Sports Medicine 4, 737–752.

Milgrom, C., Giladi, M., Stein, M., Kashtan, H., Margulies, J.Y., Chisin, R., Steinberg, R., Aharonson, Z., 1985. Stress fractures in military recruits. The Journal of Bone and Joint Surgery 67-B, 732–735.

Milner, C.E., Davis, I.S., Hamill, J., 2006a. Free moment as a predictor of tibial stress fracture in distance runners. Journal of Biomechanics 39, 2819–2825.

Milner, C.E., Ferber, R., Pollard, C.D., Hamill, J., Davis, I.S., 2006b. Biomechanical factors associated with tibial stress fractures in female runners. Medicine and Science in Sports and Exercise 38, 323–328.

Munro, C.F., Miller, D.I., Fuglevand, A.J., 1987. Ground reaction forces in running: a reexamination. Journal of Biomechanics 20, 147–155.

Niva, M.H., Kiuru, M.J., Haataja, R., Pihlajamäki, H.K., 2005. Fatigue injuries of the femur. The Journal of Bone and Joint Surgery 87-B, 1385–1390.

Novacheck, T.F., 1998. The biomechanics of running. Gait Posture 7, 77–95.

Pierrynowski, M.R., Morrison, J.B., 1985. A physiological model for the evaluation of muscle forces in human locomotion: theoretical aspects. Mathematical Biosciences 75, 69–101.

Pihlajamäki, H.K., Ruohola, J.-P., Kiuru, M.J., Visuri, T.I., 2006a. Displaced femoral neck fatigue fractures in military recruits. The Journal of Bone and Joint Surgery 88-A, 1989–1997.

Pihlajamäki, H.K., Ruohola, J.-P., Weckström, M., Kiuru, M.J., Visuri, T.I., 2006b. Long-term outcome of undisplaced fatigue fractures of the femoral neck in young male adults. The Journal of Bone and Joint Surgery 88-B, 1574–1579.

Polgár, K., Gill, H.S., Viceconti, M., Murray, D.W., O'Connor, J.J., 2003. Strain distribution within the human femur due to physiological and simplified loading: finite element analysis using the muscle standardized femur model. Proceedings of the Institution of Mechanical Engineers, Part H. Journal of Engineering in Medicine 217, 173–189.

Pollard, C.D., Davis, I.M., Hamill, J., 2004. Influence of gender on hip and knee mechanics during a randomly cued cutting maneuver. Clinical Biomechanics 19, 1022–1031.

Prilutsky, B.I., Herzog, W., Allinger, T.L., 1997. Forces in individual cat ankle extensor muscles during locomotion predicted by static optimization. Journal of Biomechanics 30, 1025–1033.

Rauh, M.J., Macera, C.A., Trone, D.W., Shaffer, R.A., Brodine, S.K., 2006. Epidemiology of stress fracture and lower-extremity overuse injury in female recruits. Medicine and Science in Sports and Exercise 38, 1571–1577.

Reilly, D.T., Burstein, A.H., 1975. The elastic and ultimate properties of compact bone tissue. Journal of Biomechanics 8, 393–405.

Sasimontonkul, S., Bay, B.K., Pavol, M.J., 2007. Bone contact forces on the distal tibia during the stance phase of running. Journal of Biomechanics 40, 3503–3509.

Schaffler, M.B., Radin, E.L., Burr, D.B., 1989. Mechanical and morphological effects of strain rate on fatigue of compact bone. Bone 10, 207–214.

Schmidt-Brudvig, T.J., 1985. Distal femoral stress fracture in military basic trainees: a report of three cases. The Journal of Orthopaedic and Sports Physical Therapy 7, 20–22.

Sullivan, D., Warren, R.F., Pavlov, H., Kelman, G., 1984. Stress fractures in 51 runners. Clinical Orthopaedics and Related Research 187, 188–192.

Taylor, S.J.G., Walker, P.S., 2001. Forces and moments telemetered from two distal femoral replacements during various activities. Journal of Biomechanics 34, 839–848.

Vaughan, C.L., Davis, B.L., O'Connor, J.C., 1992. Dynamics of Human Gait. Human Kinetics, Champaign, IL.

Visuri, T., Vara, A., Meurman, K.O.M., 1988. Displaced stress fractures of the femoral neck in young male adults: a report of twelve operative cases. The Journal of Trauma 28, 1562–1569.